Journal of Controlled Release 328 (2020) 952–961

Contents lists available at ScienceDirect

Journal of Controlled Release

journal homepage: www.elsevier.com/locate/jconrel

# Ocular barriers to retinal delivery of intravitreal liposomes: Impact of vitreoretinal interface

Shirin Tavakoli [a,*], Karen Peynshaert [b], Tatu Lajunen [a,c], Joke Devoldere [b], Eva M. del Amo [d], Marika Ruponen [d], Stefaan C. De Smedt [b], Katrien Remaut [b], Arto Urtti [a,d,e]

[a] Drug Research Programme, Division of Pharmaceutical Biosciences, Faculty of Pharmacy, University of Helsinki, Helsinki, Finland
[b] Ghent Research Group on Nanomedicines, Laboratory of General Biochemistry and Physical Pharmacy, Ghent University, Ottergemsesteenweg 460, 9000 Ghent, Belgium
[c] Laboratory of Pharmaceutical Technology, Department of Pharmaceutical Science, Tokyo University of Pharmacy & Life Sciences, 1432-1 Hachioji, 192-0392 Tokyo, Japan
[d] School of Pharmacy, Faculty of Health Sciences, University of Eastern Finland, Kuopio, Finland
[e] Institute of Chemistry, St Petersburg State University, Petergoff, St Petersburg, Russian Federation

ARTICLE INFO

*Keywords:*
Liposomes
Intravitreal
Retinal permeation
Vitreoretinal interface
Inner limiting membrane
Animal models

ABSTRACT

Drug delivery to the posterior segment of the eye is challenging due to several anatomical and physiological barriers. Thus, there is a need for prolonged action and targeted drug delivery to treat retinal diseases. Intravitreal injections avoid anterior eye barriers, but the vitreoretinal interface and inner limiting membrane (ILM) may prevent access of drug delivery systems to the retina. Existing data on retinal permeation of intravitreal nanoparticles are sparse and probably misleading due to the inter-species differences of retinal structures in rodents and humans. To bridge this gap, retinal permeation of light-activated liposomes was studied in an ex vivo bovine explant system that simulates the structure of vitreoretinal interface and intact ILM. Our findings indicate that the particle size plays a significant role in determining the retinal penetration as the liposomes of >100 nm sized failed to overcome the ILM and could not permeate into the retina. In addition, our results demonstrate the impact of surface charge and PEG-coating on retinal penetration. Small (≈ 50 nm) anionic liposomes with PEG coating showed the most extensive distribution and cellular localization in the retina. In summary, this study extends understanding of ocular barriers, and provides valuable information to augment design of retinal drug delivery systems.

## 1. Introduction

Disease-related retinal damage is the leading cause of visual impairment and blindness in industrialized countries, imposing a huge burden on the economy and quality of patients' lives [1,2]. The most prevalent posterior segment eye diseases are age-related and the number of patients suffering from such disorders increases with the aging of the global population [3,4]. Treatment of retinal diseases, such as age-related macular degeneration (AMD), diabetic retinopathy (DR) and glaucomatous retinal degeneration, is still challenging and new treatments are needed. Retinal drug delivery is hampered by several ocular barriers (e.g. blood retinal barrier). Thus, retinal diseases cannot be treated by topical, systemic or periocular (e.g. sub-conjunctival and peribulbar) routes of administration, since adequate drug concentrations are not achieved in the retina.

Intraocular modes of drug administration, such as intravitreal, subretinal and suprachoroidal injections, are used in retinal drug delivery, but only intravitreal (IVT) injections are in worldwide clinical use [5]. IVT injections are used routinely in the anti-vascular endothelial growth factor (anti-VEGF) treatment of exudative age-related macular degeneration, representing 80.6% of the retinal therapeutics market (Market Scope Estimate, http://market-scope.com/). Clinically accepted IVT injections offer several advantages: 1) the drug is injected directly into the vitreous humour, resulting in retinal delivery, 2) the injections bypass several ocular barriers (e.g. blood-retinal barrier, blood-aqueous barriers, cornea, sclera), and 3) reduced systemic side effects. However, the injectable solutions require frequent IVT dosing that is problematic for the patients and healthcare system. The acceptable injection interval

* Corresponding author.
*E-mail address:* shirin.tavakoli@helsinki.fi (S. Tavakoli).

https://doi.org/10.1016/j.jconrel.2020.10.028
Received 24 July 2020; Received in revised form 15 October 2020; Accepted 16 October 2020
Available online 19 October 2020

depends on the disease state: in serious disease states (e.g. wet AMD) more frequent drug administrations can be accepted than in slowly progressing early stage disease (e.g. dry AMD). The injection intervals of anti-VEGF antibodies (e.g. bevacizumab) are 1–2 months which leads to reduced patient compliance and sub-optimal treatment outcomes. In the case of small molecule drugs, the dosing intervals would be too short (a few days) for clinical purposes as the intravitreal half-lives of small molecules are usually less than 10 h [6]. There is an unmet need to develop retinal drug delivery systems with prolonged injection intervals and effective retinal permeation.

Over the last decades, numerous viral and non-viral nanoparticles have been investigated for retinal delivery of drugs and genes [7–10]. Currently, sub-retinal injections are considered to be the most effective mode of retinal nanoparticle delivery, but these injections are much more demanding in clinical practice than IVT delivery. The sub-retinal injections are not widely accepted in the clinical practice and may never become widely used in the clinics. Effective IVT delivery of nanoparticles to the retina may enable wide clinical use of viral and non-viral therapeutics in the retinal diseases.

Currently, retinal delivery of IVT nanocarriers is hindered by two barriers: vitreous and vitreoretinal interface (Fig. 1). The vitreous is a highly hydrated gel-like matrix of intertwined collagen fibres and glycosaminoglycans [11,12]. Collagen fibrils maintain the gel state of the vitreous, whereas hyaluronic acid provides the swelling pressure by its charged carbohydrate chains that attract water and counter ions [13,14]. The vitreous humour restricts mobility of nanoparticles and the most pronounced effects are seen with cationic nanocarriers [15–19]. Overall, particle characteristics are important for their mobility in the vitreous [15].

Vitreoretinal interface limits material permeation from the vitreous into the retinal layers. This interface is composed of 1) cortical vitreous, 2) inner limiting membrane (ILM) (the innermost boundary of the retina) and 3) expanded Müller cell footplates [20]. Cortical vitreous with high collagen concentration is a thin layer (100–300 μm) that runs parallel to the ILM [14]. Müller cells are glial cells which span throughout the retina from vitreal side to the distal side of the outer nuclear layer [5,8]. The major components of ILM are collagen type IV, laminin and fibronectin, but the composition and thickness varies among species and disease states [11,20–22]. ILM forms a physical barrier at the vitreoretinal interface [16,23]. Several studies have reported viral and non-viral gene delivery to the retinal targets in rodents [23–25], but the ILM in mice, and rats is thin (<0.1 μm) resembling foetal human ILM [22]. Therefore, the results from rodent eyes are not representative for retinal drug delivery in larger species with different ILM structure. Thus, improved understanding of retinal permeation of nanoparticles is needed.

In this study, we investigated systematically the retinal permeation of nanoparticles in bovine eyes. Liposomes were used, since they are well-documented nanoparticles for drug and gene delivery. We studied the retinal penetration of light-activated liposomes that are based on the use of indocyanine green (ICG) as triggering agent for light activated drug release [26]. Given the promising vitreal mobility of anionic and neutral liposomes [15], we evaluated how properties of such liposomes (particle size, surface charge, surface coating) affect their retinal permeation. Two types of ex vivo bovine explants were used: retinal model without vitreous and vitreoretinal explant with intact entire vitreoretinal interface as developed by Peynshaert et al. [27]. Herein, we report the features that determined the permeation of liposomes through vitreoretinal interface. This information helps the design of retinal drug delivery systems.

## 2. Materials and methods

### 2.1. Materials

1,2-Distearoyl-sn-glycero-3-phosphoglycerol (DSPG), 1,2-dipalmitoyl-sn-glycero-3-phosphocholine (DPPC), 1,2-distearoyl-sn-glycero-3-phosphocholine (DSPC), 1-stearoyl-2-hydroxy-sn-glycero-3-phosphocholine (Lyso PC), 1,2-distearoyl-sn-glycero-3 phosphoethanolamine (DSPE), 1,2-distearoyl-sn-glycero-3-phosphoethanolamine-N-[methoxy (polyethylene glycol)-2000] (DSPE-PEG), 1,2-dioleoyl-3-trimethylammonium-propane (DOTAP) and 1,2-dioleoyl-*sn*-glycero-3-phosphoethanolamine-*N*-Cyanine 5 (Cy5-PE) were purchased from Avanti Polar Lipids, Inc. (Alabaster, AL, USA). The extruder was from Avanti Polar Lipids (Alabaster, AL, USA) and the 30 nm, 50 nm and 100 nm, Nuclepore® polycarbonate membranes (diameter 19 mm) were bought from Whatman Int. Ltd. (Maidstone, England). 75 mm Transwell® with 0.4 μm Pore Polycarbonate Membrane Insert (3419) was obtained from Corning™. Disposable base molds (41742) were acquired from Shamdon™. Biopsy punch (10 mm) was purchased from Robbins Instruments, Catham, US. Anti-Collagen IV antibody (ab6586) was purchased from Abcam. Hoechst (33342) and AlexaFluor® 488 labelled secondary antibody (A11034) was provided from Invitrogen™, USA. Tissue culture materials were from Gibco™: Neurobasal®-A medium (10888022), carbon dioxide independent medium (18045088), B-27® supplement (17504044), Penicillin-streptomycin (15140122), L-Glutamine

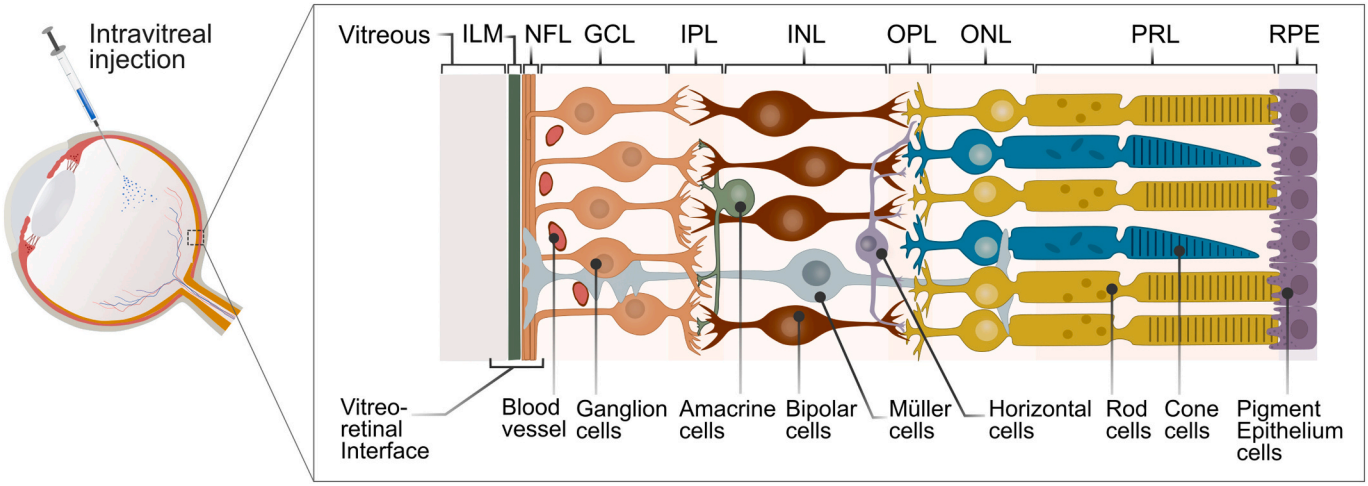


**Fig. 1.** Schematic representation of the eye with detailed retinal structure. Vitreous and vitreoretinal interface are the first barriers to retinal delivery of nanoparticles after intravitreal injection. Retinal layers: inner limiting membrane (ILM), nerve fibre layer (NFL), ganglion cell layer (GCL), inner plexiform layer (IPL), inner nuclear layer (INL), outer plexiform layer (OPL), outer nuclear layer (ONL), photoreceptors layer (PRL), retinal pigment epithelium (RPE).

(25030081). Chloroform and methanol used in the lipid stock solutions, HEPES (4- (2-hydroxyethyl) piperazine-1-ethanesulfonic acid) were purchased from Sigma-Aldrich. All reagents were analytical grade.

### 2.2. Liposome preparation

Lipids (10 μmol) at various molar ratios (Table 1) were dissolved in chloroform prior to liposome preparation. Liposomes were formulated by thin film hydration method followed by extrusion as previously reported [15]. In brief, lipid mixture solutions were placed in rotary evaporator to remove the organic solvent at 65 °C under nitrogen flow condition by gradually reducing the pressure below 100 mbar. The thin lipid film was formed and hydrated by 500 μl of HEPES buffer saline solution (20 mM HEPES and 140 mM NaCl, pH 7.4) in water bath at the same temperature. Liposomes were then extruded 11 times at 65 °C through polycarbonate filter membranes with the pore size of 30 and 50 or 100 nm using a syringe-type mini-extruder followed by immediate cooling down and stored at 4 °C. In anionic liposome preparation, DSPC was partially replaced by DSPG to have the final 10% molar ratio of negatively charged lipid in the lipid composition. Indocyanine green (ICG) at 1:50 molar ratio (to total lipids) was integrated in the lipid bilayer by dissolving ICG in methanol and adding it to the lipid mixture in chloroform prior to evaporation of the organic solvent. EE% of ICG was not measured due to the rapid degradation of non-capsulated ICG in aqueous solution; however, our previous molecular dynamics simulations [26] indicate that ICG strongly prefers to be localized in the lipid bilayer indicating probable high EE%. Cy5-PE (0.5 mol%) was applied to label the liposomes.

### 2.3. Particle size and ζ-potential analysis

The particle size was measured by dynamic light scattering (DLS) using Malvern Zetasizer APS automated plate sampler (Malvern Instruments Ltd., Malvern, United Kingdom). Data acquisition was performed with Malvern DTS v7.01 software and the result were reported as size distribution by particle number and polydispersity index. Prior to measurement, each sample was diluted at 1:10 *v*/v ratio in HEPES buffer (pH 7.4) and analysed three times with 13 sub-runs. The zeta potential was determined using the same dilution ratio at room temperature with a Zetasizer ZS v7.1.1 (Malvern Instruments Ltd.).

### 2.4. Preparation of bovine retinal explant without vitreous (R-explant)

Fresh bovine eyes were provided by a local abattoir and transported in cold carbon dioxide ($CO_2$) independent medium. Extra-ocular connective tissues were removed and the eyes were shortly immersed in 20% ethanol and kept in 4 °C $CO_2$ independent medium until dissection. The sclera was punctured approximately 10 mm below the limbus using 21 G needle and cut circumferentially with curved surgical scissors. The vitreous was gently removed and the posterior eyecup was filled with cold medium in order to avoid drying. The eyecup was then cut along the large veins in order to obtain 4 flaps while submerging the whole structure in medium. Next, a biopsy punch (10 mm) was used to cut circular pieces of retina from each flap followed by gentle pipetting of the medium underneath the cut surface, thus allowing isolation of the retina. Two retinal explants were transferred to 75 mm Transwell® insert and placed on the filter with photoreceptors facing down (Fig. S1). The explants were nourished by adding 10 ml of medium below the filter (Neurobasal®-A medium supplemented with 2% L-Glutamine, 1% B-27® supplement and 2% Penicillin-streptomycin).

### 2.5. Preparation of vitreoretinal bovine retinal explant (VR-explant)

The VR-explant with attached vitreous was prepared as described earlier [27]. This method maintains the intact ILM during the preparation. Briefly, after removal of extraocular tissues, the eyes were transferred to a beaker with $CO_2$ independent medium at room temperature and, thereafter, incubated for 10 min in a 37 °C water bath. Such incubation period is essential as it facilitates the smooth separation of retina from the RPE-choroid while maintaining attached vitreous on the retina. The eye was dissected as explained above, but unlike the R-explant, the vitreous gel was retained in the posterior eyecup. Next, the retina with vitreous was gently separated from the choroid at the edge of the eyecup toward the optic nerve. The whole structure was then slid into a petri dish filled with 4 °C $CO_2$ independent medium (the vitreous facing upwards). VR-explants were cut into several pieces (around 1.5 $cm^2$) with a surgical blade while they were submerged in the medium. Each explant was then transferred to a 75 mm Transwell® filter followed by addition of the supplemented Neurobasal®-A medium under the filter (Fig. S1). Finally, excess of vitreous gel, adjacent to the explant, was aspirated with Pasteur pipette and removed by scissors so that the explant was ready for IVT injections of liposomes.

### 2.6. Retinal explant treatment with liposomes

The explants were treated with liposomes immediately after preparation. In R-explant, 10 μl of labelled liposome (3 mg/ml) was placed carefully on top of the retinal explant in order to assure that the formulation covers the explant sufficiently without overflow across the edges. Given the vitreous is attached to the retina in the VR-explant, the liposome solution (7 mg/ml) was injected intravitreally into this model. Four injections of 50 μl were performed horizontally to avoid retinal damage and prevent direct delivery of the particles into the retina. Transwells® were then placed in the incubator with 5% $CO_2$ at 37 °C and incubated for 24 h or 48 h.

### 2.7. Cryosectioning, immunohistochemistry and imaging

After the incubation period, retinal explants were fixed by cutting out the Transwell® filter surrounding the explant, placing the filter with explant attached in a 6-well plate with 4% paraformaldehyde (PFA) and incubating the explants for 2 h at 4 °C.

**Table 1**
Lipid composition, associated molar ratios and physicochemical properties of ICG-liposomes. The formulations are categorized based on the particle size and surface charge (A: anionic and N: neutral).

| Formulation | | Lipid composition | Molar ratios | Size (nm) | PdI | ζ-Potential (mV) |
|---|---|---|---|---|---|---|
| ≤50 nm | | | | | | |
| Anionic | A1-PEG | DPPC:DSPG: Lyso-PC:DSPC:DSPE-PEG:ICG | 75:10:10:5:4:2 | 41.5 ± 7.7 | 0.182 | −28.2 |
| | A2 | DPPC:DSPG:Lyso-PC:DSPC:DSPE:ICG | 75:10:10:5:4:2 | 48.1 ± 4.9 | 0.107 | −36.8 |
| Neutral | N1-PEG | DPPC:DSPC:Lyso-PC:DSPE-PEG:ICG | 75:15:10:4:2 | 56.3 ± 5.5 | 0.211 | −3.1 |
| | N2 | DPPC:DSPC:Lyso-PC:DSPE:ICG | 75:15:10:4:2 | 51.32 ± 14.2 | 0.138 | −7.7 |
| ≥100 nm | | | | | | |
| Anionic | A3-PEG | DPPC:DSPG:Lyso-PC:DSPC:DSPE-PEG:ICG | 75:10:10:5:4:2 | 107.2 ± 6.5 | 0.053 | −27.6 |
| | A4 | DPPC:DSPG:Lyso-PC:DSPC:DSPE:ICG | 75:10:10:5:4:2 | 100.7 ± 1.1 | 0.039 | −57.9 |
| Neutral | N3-PEG | DPPC:DSPC:Lyso-PC:DSPE-PEG:ICG | 75:15:10:4:2 | 113.1 ± 14.3 | 0.068 | −3.4 |
| | N4 | DPPC:DSPC:Lyso-PC:DSPE:ICG | 75:15:10:4:2 | 112.6 ± 8.8 | 0.042 | −6.7 |

Thereafter, the fixative was discarded and the explants were cryopreserved following this scheme: 30% sucrose (overnight, 4 °C); a 1:1 solution of Tissue-Tek® O.C.T/30% sucrose (3 h, 4 °C); pure O.C.T (3 h; room temperature). This special cryopreservation protocol was developed to prevent separation of the vitreous layer from the retinal tissue during cryosection cutting. After cryopreservation the explants were transferred to cryomolds, embedded in fresh O.C.T and snap frozen by submerging the cryomolds in isopentane cooled with dry ice. Subsequently, cryoblocks were removed from the mold and cut at a thickness of 16 μm with a cryostat (Leica CM3050s). Cryosections were obtained from 4 different explant sites. From each location, 6 sections were prepared to obtain 24 cryosections per explant.

To stain the retinal sections, 5% goat serum in PBS was prepared as a blocking solution. Next, each section was incubated in 50 μl of blocking solution for 1 h at room temperature followed by overnight incubation with rabbit anti-collagen IV antibody (50 μl, 1:200) at 4 °C. The sections were then labelled with Alexa Fluor™ 488-tagged goat anti-rabbit secondary antibody (50 μl, 1:500) and Hoechst at 10 μg/ml for 1 h at room temperature. Lastly, retinal sections were mounted in antifade mounting medium (Vectashield®, Vector Laboratories, CA, US) and stored at 4 °C until imaging. Visualization and imaging were performed with a confocal microscope (Leica TCS SP8) using 20× (HC PL APO 20×/0.75 IMM CORR CS2) and 93× (HC PL APO 93×/1.30 mot CORR STED WHITE) objectives.

Images were analysed by FIJI (imageJ 1.51, NIH) and the number of particles for the semi-quantitative analyses were counted according to a reported method [27]. Descriptive statistical analysis was performed using GraphPad Prism 8.2.1 in order to define quartiles of the data (median, 25th and 75th percentile). Accordingly, we categorized the retinal penetration into high, moderate and low levels, based on the number of liposomes per 1000 $\mu m^2$ of retinal section: high ($> 42$), moderate (7–42) and low ($< 7$) per region of interest.

## 3. Results

### 3.1. Characterization of liposomes

The physicochemical properties of liposomes including lipid composition, hydrodynamic diameter (size), the polydispersity index (PdI), and the ζ -potential are presented in Table 1. Surface charge (ζ -potential) was altered by changing the lipid composition. ICG-liposomes showed similar values of particle size and ζ -potential measurements comparing to the controls [15]; hence, ICG did not have significant effect on physicochemical characteristic of the particles. Likewise, we did not observe any difference in particle size and surface charge between Cy5-labelled and unlabelled liposomes. Liposomal formulations had homogenous distribution (PdI $< 0.2$).

### 3.2. Effect of nanoparticle surface on their retinal distribution

As anionic and neutral liposomes diffuse freely in the vitreous humour [15], we investigated their retinal penetration using bovine retinal explant models. The liposomes were categorized based on PEG coating, size, and surface charge (Table 1).

Firstly, the liposomes were applied on conventional retinal explants ("R-explant") without vitreous humour. Thereafter, the VR-explant with the vitreous attached to the retina was applied for the permeation study to rule out the possible influence of ILM damage during the removal of the vitreous. Our data shows that PEGylated (A1-PEG, N1-PEG) small liposomes (41.5 nm and 56.3 nm, respectively) successfully entered the retina in R-explant (Fig. S2). These liposomes were further investigated with the VR-explants. Since retinal permeation showed differences among explants and regions within one explant, at least 32 images were analysed to validate the results in Fig. 2. Both anionic (A1-PEG) and neutral (N1-PEG) liposomes permeated through retinal layers, but the distribution of the liposomes was not even in all layers and they were mostly located in the inner retina. We also observed the signs of cell localization of liposomes in ganglion cell layer (GCL) (Fig. 2B). According to the semi-quantitative analysis, retinal penetration of anionic liposomes (A1-PEG) was moderately higher than that of neutral liposomes (N1-PEG).

To examine the effect of surface coating on the retinal transfer, we compared the non-PEGylated and PEGylated anionic and neutral liposomes within the same size range ($< 50$ nm). In R-explant, both liposomes showed comparable retinal penetration, as they were able to reach and migrate throughout the inner retinal layers, but the distribution seems to be restricted within GCL (Fig. S2, Fig. 3A: R-explant). In VR-explant, we saw variations between retinal sections that were incubated with liposomes devoid of PEG suggesting less efficient retinal permeation as compared with PEGylated liposomes (Figs. 2–3). Even though some retinal sections showed permeation of A2 and N2, the retinal distribution was less consistent than with PEGylated liposomes (Fig. 3A–B). In conclusion, PEG-coating facilitates retinal permeation of the liposomes.

### 3.3. Effect of liposome size on retinal distribution

Next, we studied the permeation of differently sized liposomes into the bovine explants. First, R-explants were used. Here, we investigated the retinal transfer of anionic PEGylated (A3-PEG), anionic non-PEGylated (A4), neutral PEGylated (N3-PEG) and neutral non-PEGylated (N4) liposomes with a size range $\geq$ 100 nm (Table 1). Regardless of surface coating and charge these liposomes failed in crossing the ILM barrier and retinal entry (Fig. 4). Interestingly, the retinal penetration of larger liposomes was only detected in the cryosections with compromised ILM implying the barrier role of ILM (Fig. S3).

### 3.4. Influence of incubation time on retinal distribution of liposomes

Although 24 h of incubation seemed sufficient for the liposomes to be taken up by the ex vivo R and VR-explants, we examined the influence of prolonged exposure. Retinal distribution of small anionic PEG-coated liposomes (A1-PEG) was studied after 48 h of incubation on VR bovine explant. Cryosection images showed higher extent of retinal penetration. This was seen as reduced brightness in the vitreous and ILM, suggesting lower level of liposome entrapment in the ILM. Compared to the limited number of PEGylated liposomes in outer retinal layer after 24 h (Fig. 2A), more liposomes migrated to the deeper retinal layers and the outer retina during 48 h (Fig. 5). Moreover, a detailed confocal image at higher magnification (Fig. 5 bottom row) shows again co-localization of liposomes with ganglion cells.

In the experiment, ≈100 nm anionic and PEGylated liposomes (A3-PEG) were studied with ex vivo retinal R-explant for 48 h to investigate their possible retinal permeation during longer time. However, the results did not show any retinal transfer even after 48 h (Fig. 6) indicating that vitreoretinal interface blocks the retinal transfer of liposomes with the particle size of over 100 nm.

## 4. Discussion

Visual impairment and blindness are caused by various retinal diseases, but the delivery of therapeutics to the retina is limited by the anatomical and physiological barriers. The most common retinal therapies involve IVT injections of steroids [28] and anti-VEGF antibodies [29,30]. These treatments involve frequent IVT injections on chronic basis. For corticosteroids, IVT implants have been used for prolonged IVT dosing intervals, but with exception of few explants such as Ozurdex®, they have not gained wide clinical use. Consequently, alternative approaches are needed to prolong the dosing intervals and to enable retinal targeting of IVT therapeutics. IVT injected nanoparticles may prolong ocular drug retention and provide sustained drug delivery to the

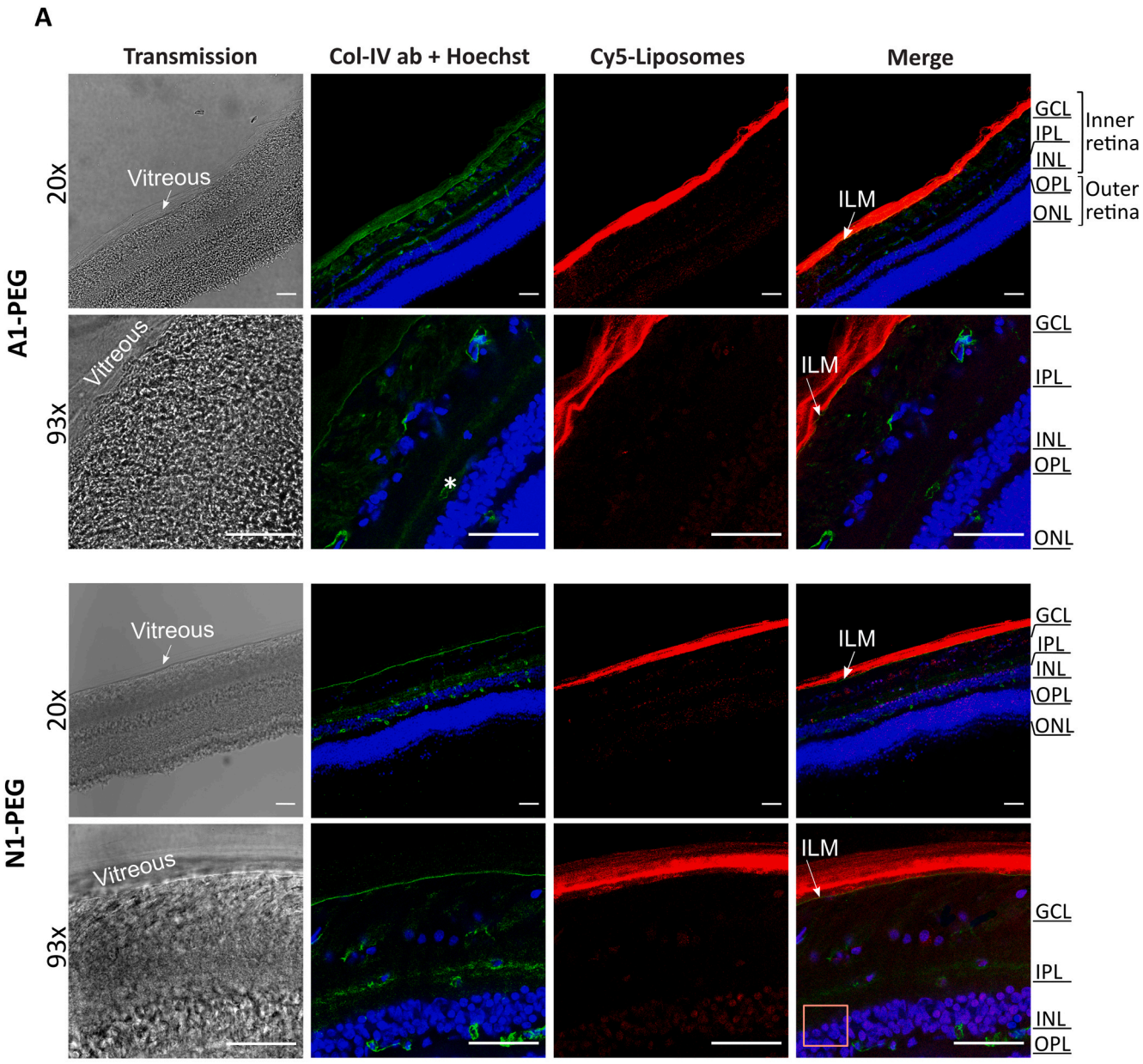


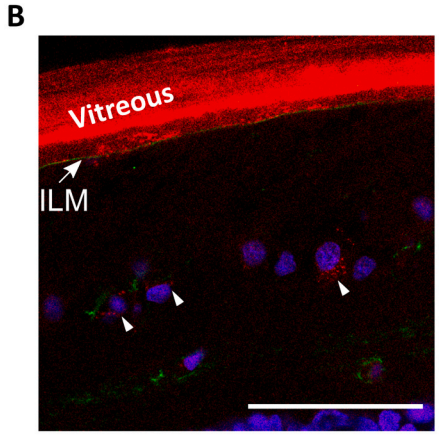


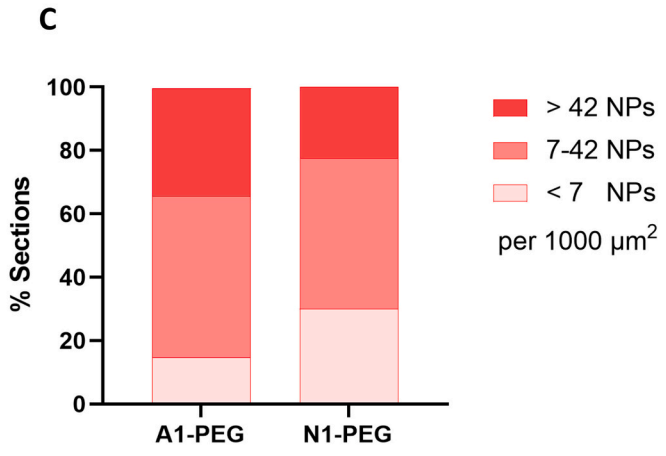


(caption on next page)

**Fig. 2.** Retinal distribution of PEGylated negatively charged (A1-PEG) and neutral (N1-PEG) ≈ 50 nm liposomes in bovine vitreoretinal explant 24 h post-IVT injection. (A) Representative confocal microscopy images of cryosections displaying the permeation of Cy5-labelled A1-PEG and N1-PEG in retinal layers (red). The ILM is labelled with anti-collagen type IV antibody (green) which also stains the retinal blood vessels, highlighted with " * ". The vitreous can be seen as transparent layer in transmission imaging which is well aligned along the ILM while it appears in bright red colour due to the high load of Cy5-labelled particles in merged channel mode. Nuclei are stained with Hoechst (blue). (B) Representative image of retinal cross-section at higher magnification showing the co-localization of liposomes with ganglion cells (highlighted with white arrowheads). Scale bar: 50 μm. (C) Semi-quantitative analysis of retinal distribution of neutral and anionic PEGylated liposomes in vitreoretinal explant after 24 h of incubation. The numbers refer to the liposomes within the region of interest (1000 $\mu m^2$) ($n = 3$). (For interpretation of the references to colour in this figure legend, the reader is referred to the web version of this article.)

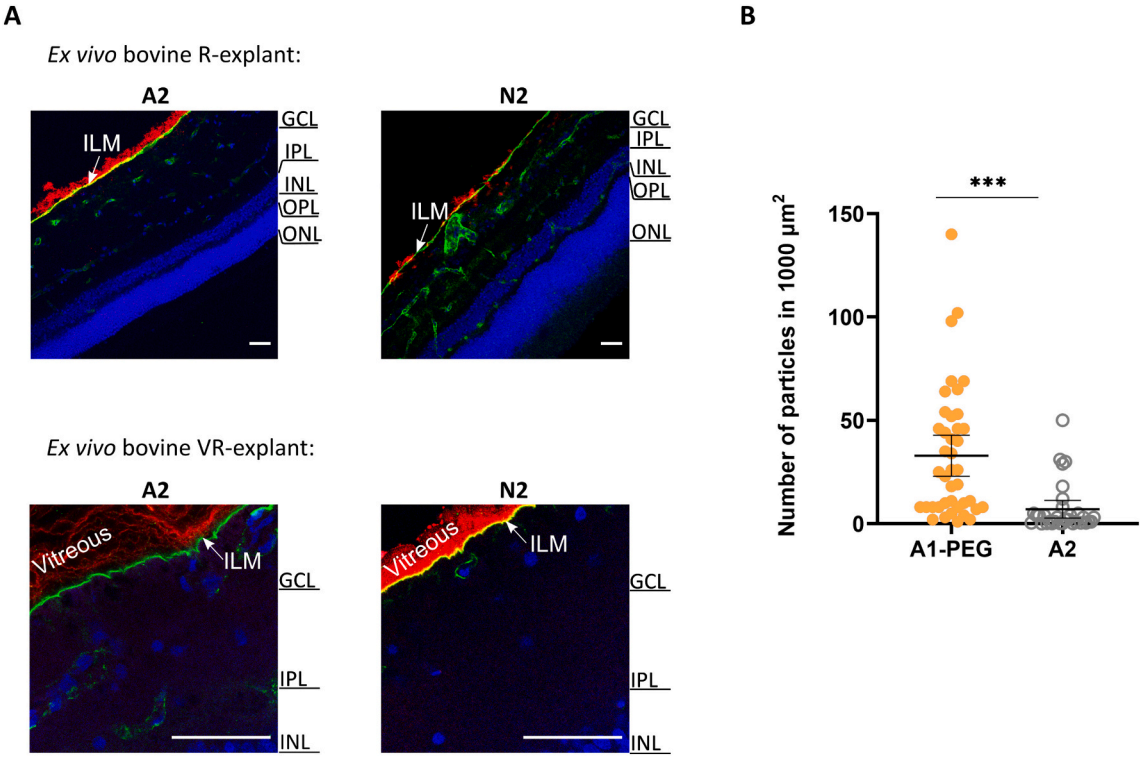


**Fig. 3.** (A) Representative cryosection images showing the retinal distribution of non-PEGylated liposomes in ex vivo bovine explants. The confocal microscopy images of VR-explants demonstrate retinal sections without retinal permeation of liposomes. ILM and retinal blood vessels are stained with anti-collagen type IV antibody (green), the nuclei are stained with Hoechst (blue) and particles labelled with Cy5 are shown in red. Scale bar: 50 μm. (B) Semi-quantitative analysis of retinal transfer across the ILM comparing the distribution of anionic PEGylated and non-PEGylated liposomes in vitreoretinal explants after 24 h of incubation. *P* value <0.001 by an unpaired *t*-test. ($n = 3$). (For interpretation of the references to colour in this figure legend, the reader is referred to the web version of this article.)

retinal targets. Recently, we developed ICG-containing light-activated liposomes that allow spatial and temporal control of contents release [26]. This approach is interesting for the controlled drug delivery into the retina. Nonetheless, for the effective retinal therapy, liposomes must permeate successfully from the vitreous to the retina. Previously, we showed the impact of physical-chemical features on vitreal mobility of lipid-based nanostructures (e.g. liposomes) [15]. As anionic and neutral liposomes, with and without ICG, permeate easily in the vitreous, we investigated their ability to cross the vitreoretinal interface. We did not include cationic liposomes in this study, because the positive charge limits the vitreal mobility of particles [15–17,19]. Furthermore, their permeation across the vitreoretinal interface is blocked by their interactions with negatively charged ILM components, such as heparan sulphate [23,31,32].

Previous studies have reported successful retinal delivery of viral and non-viral nanocarriers, but these experiments were conducted mostly in rodents (rats, mice) that have thinner ILM than larger animals and humans [22,33]. Therefore, we applied bovine retinal explants to obtain more relevant and systematic data on retinal permeation of liposomes. The bovine vitreous is comparable to its human counterpart [19,34–36] and the thickness of bovine ILM is similar with the adult human and non-human primate ILM (the thickness can reach up to 4 μm in posterior pole based on atomic force microscopic images) [21,27,33,37,38]. These are very different values from the ILM thickness in adult mouse (< 0.1 μm) and human foetus (≈ 0.07 μm) [21,31,33,39].

The barrier role of ILM was demonstrated in this study, also in the experiments with broken explant ILM (Fig. S3). In those cases, even 100 nm liposomes distributed to the retina. The structure of the ILM may also be influenced by age and retinal degeneration [40]. In some diseases, such as diabetic retinopathy, increased permeability of ILM has been observed. Even though disease-induced leakiness of ILM might increase retinal permeation of nanoparticles, this situation may be relevant only in the case of late-stage severe disease. As there are numerous retinal diseases and levels of their seriousness, the issue of disease state vs permeation is fragmented and complicated. To make robust retinal delivery system, applicable to many diseases and their different stages, one should not rely on hypothetical enhanced permeability across ILM, but rather develop a delivery system that would permeate even through the intact ILM. Overall, we are convinced that our data herein is translationally more relevant than the previous published rodent data.

Our work showed that anionic and neutral liposomes of ≈50 nm penetrate into the retina and distribute in the inner retina, and to some

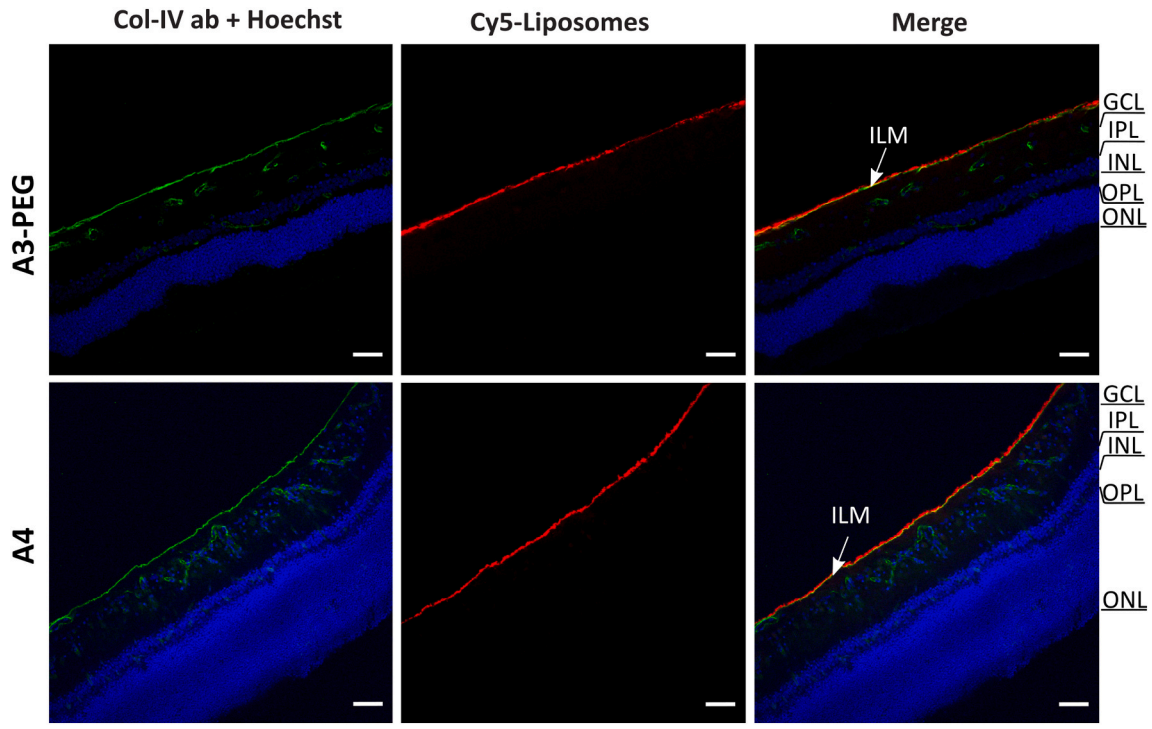


**Fig. 4.** Representative cryosection images display the failure in retinal distribution of PEGylated (upper row) and non-PEGylated anionic formulations (bottom row) of ≥100 nm liposomes in ex vivo bovine R-explants. ILM and retinal blood vessels were visualized by staining with anti-collagen type IV antibody (green), the nuclei were labelled with Hoechst (blue), and Cy5-liposomes are shown in red. Scale bar: 50 μm. ($n = 3$). (For interpretation of the references to colour in this figure legend, the reader is referred to the web version of this article.)

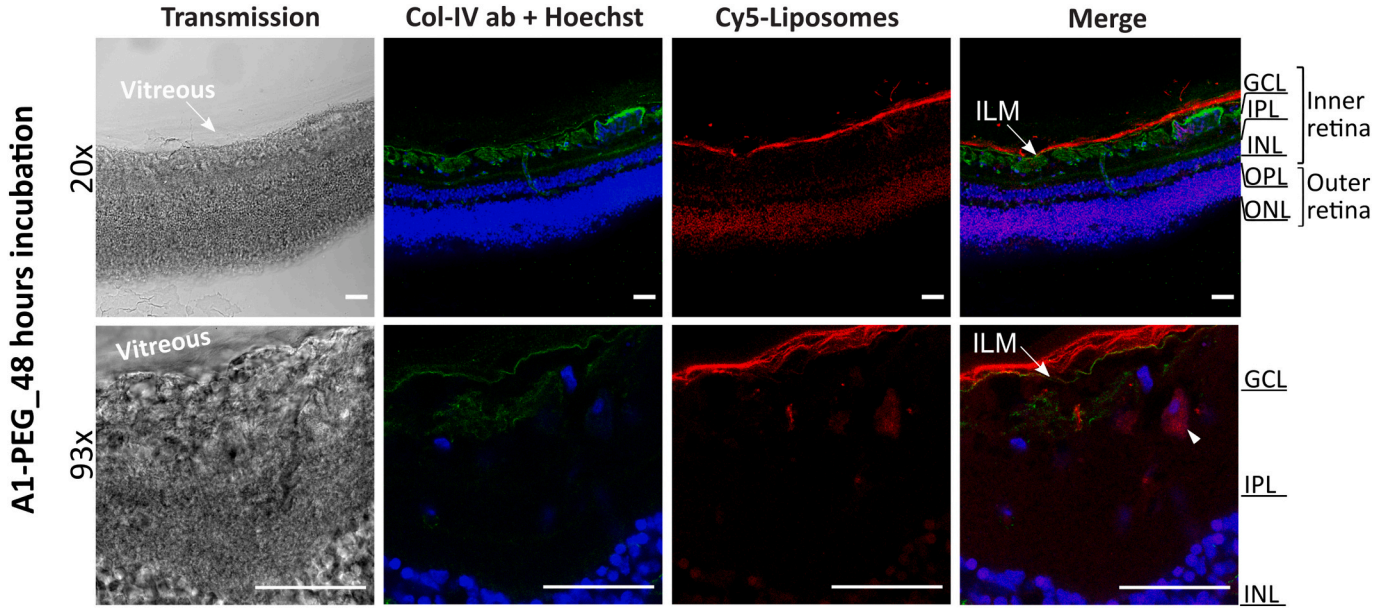


**Fig. 5.** Representative distribution of PEGylated anionic liposomes (A1-PEG) throughout the retinal layers 48 h post-IVT injection in ex vivo bovine VR-explant. Cryosection images show the localization of liposomes in inner and outer retina. At 93× magnified confocal image, localization of liposomes in a ganglion cell is evident (highlighted with white triangle). ILM was stained with anti-collagen type IV antibody (green) which also labels the retinal blood vessels, nuclei were stained with Hoechst (blue) and Cy5-liposomes are displayed in red. Scale bar: 50 μm. ($n = 3$). (For interpretation of the references to colour in this figure legend, the reader is referred to the web version of this article.)

extent also in the outer retinal layers (Fig. 2A). However, larger liposomes (≈100 nm) were not able to cross vitreoretinal interface, suggesting that the mesh size of the ILM may be between 50 nm and 100 nm, which is in line with previously shown hampered permeation of polystyrene bead (100 and 200 nm) into the bovine retina [27]. It is worth mentioning that the particle size distribution of the liposomes is narrow (PdI < 0.2) and our recent proteomics data shows that the protein corona results in only 10–12% increase in the liposome size in the vitreous [15]. The mesh size in the bovine ILM seems to be much smaller than the mesh size in the vitreous (≈500 nm) [19] or the sizes of

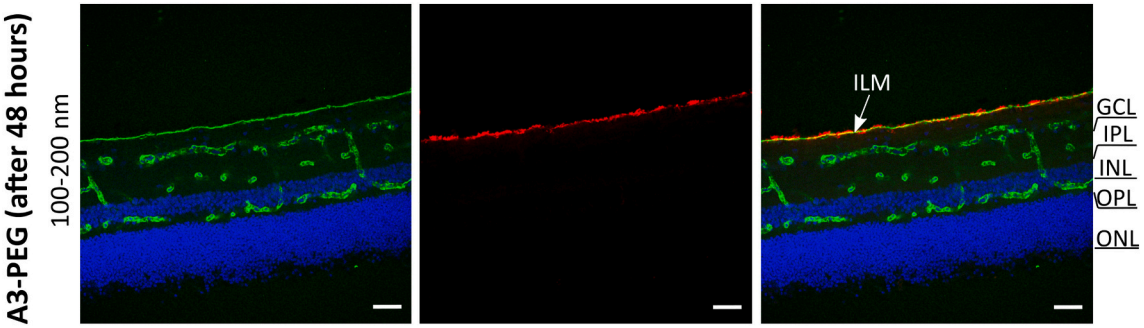


**Fig. 6.** Representative retinal cryosection images showing the hindered distribution of PEGylated anionic liposomes with a particle size of over 100 nm after incubation for 48 h in ex vivo bovine R-explant. ILM and retinal blood vessels was stained with anti-collagen type IV antibody (green), nuclei were stained with Hoechst (blue) and liposomes are labelled with Cy5 (red). Scale bar: 50 μm. (n = 3). (For interpretation of the references to colour in this figure legend, the reader is referred to the web version of this article.)

particles that permeate across the vitreoretinal surface of rodents (100–420 nm) [9,23,41–44]. Our observations are attributed to denser structure of ILM and high concentration of hyaluronic acid in cortical vitreous [20,39]. The mesh size in bovine and human ILM have been reported to be similar although the bovine vitreous is more viscous compared to human vitreous [45], further supporting the translational value of this study.

Our results clearly demonstrate more consistent retinal permeation of PEG-coated liposomes, as compared to the liposomes without PEG. Particularly in the case of non-PEGylated liposomes, substantial variation was seen in liposome permeation to the VR-explant. Apparently, hydrophilic PEG coating somehow reduces liposome binding with ILM, thereby facilitating retinal distribution. Previously, it was reported that the PEG coating with a molecular weight of ≥2 kDa facilitates the transport of nanoparticles across the mucosal barrier [46]. Given the similar structural component of vitreous/ILM to mucous (negatively charged polysaccharide network in water), higher retinal penetration of PEG-coated particles may be attributed to the same mechanism. Nonetheless, there are only limited data about the PEG effects on the retinal permeation. Previously, positive impact of hyaluronic acid coating on nanoparticle's distribution into the retina was shown, which support this hypothesis according the superior penetration of hyaluronic acid-coated nanoparticles compared to the non-coated counterparts. Large hyaluronic acid-coated liposomes, however, failed to permeate into the retina [47]. Therefore, both coating and particle size are important determinants of retinal particle permeation across the ILM.

Cellular interactions of nanoparticles, such as liposomes, within the retina are an interesting but sparsely studied phenomenon. In principle, Müller cells could serve as an avenue for nanoparticle transfer from the inner retina to the outer retina, if the particles are transported within these cells and exocytosed in the outer retina. Anionic particles have higher interaction with Müller cells than the neutral particles [23], possibly contributing to the moderately improved retinal penetration of anionic liposomes (Fig. 2C). Previously, higher phagocytic uptake of charged particles as compare to the neutral ones was shown in the Müller cells [23,49]. Such a mechanism was suggested previously for retinal distribution of intravitreal nanoparticles [7,50]. Intercellular communication of retinal cells with extracellular vesicles might also contribute to the distribution of liposomes [3,44]. Interestingly, we observed co-localization of light-activated liposomes (< 50 nm) with ganglion cells (Figs. 2 and 5). Targeted delivery to ganglion cells may have important implications in the treatment of glaucomatous retinal degeneration, since these cells play a key role in the retinal pathology of glaucoma [48].

We demonstrate here the impact of liposomal surface coating, charge and size on their retinal permeation. In addition, other factors may affect liposomal retinal distribution, but they are poorly known. Distribution of small liposomes into the deep retina (see outer nuclear layer in Fig. 5) could be attributed to the short hydrocarbon chain length (e.g. DPPC) in the light-activated liposomes. Short hydrocarbon chains and lyso-PC yield more fluid bilayers [26,51] that may facilitate cellular uptake and biological transport in the retina. Moreover, the particle shape may influence retinal permeation through sieve-like ILM. Accordingly, retinal permeation of tubular polymeric nanoparticles was shown recently in bovine retina [52].

Overall, retinal particle penetration is a multifactorial process in which ILM plays an important role. The factors include nanoparticle characteristics and endogenous factors, such as cellular activity, age- and disease related changes, and regional morphological differences. In this regard, our data provide systematic data on the effects of liposomal characteristics on ILM permeation, also demonstrating that the bovine explant model is much tighter than previously published rodent models. Thus, we believe that this study is a step forward in understanding the barrier properties at vitreoretinal interface.

## 5. Conclusions

We characterized liposomal permeation from the vitreal side to the retina in bovine explant models. Compared to the vitreal barrier, the vitreoretinal interface and the ILM represent significant barriers for particle penetration. Our data indicate that small liposomes (≈50 nm) permeate to the retina, whereas larger liposomes (≈100 nm) do not. Furthermore, PEGylation and anionic surface charge are beneficial for retinal liposome distribution. Our results indicate that the vitreoretinal interface is stronger barrier than previously thought based on the rodent studies. However, more in-depth investigations are needed to elucidate the roles of different cells in liposome localization in the retina. In conclusion, our observations highlight the importance of employing representative animal models in retinal distribution studies and provides systematic understanding on the roles of particle characteristics in retinal liposome permeation.

*Acknowledgement*

Shirin Tavakoli, Arto Urtti and Stefaan de Smedt acknowledge the research support from European Union's Horizon 2020 research and innovation program Marie Sklodowska-Curie Innovative Training Networks (ITN) NANOMED (grant no. 676137). Grant support from Russian Government Mega-Grant14.W03.031.0025 "Biohybrid technologies for modern biomedicine" to Arto Urtti is acknowledged. Tatu Lajunen acknowledges additional support from Business Finland (#4208/31/2015), Orion Research Foundation (#9-8214-9), Phospholipid Research Center, Instrumentarium Science Foundation and Silmäsäätiöiden Tohtoritutkijapooli and Eva del Amo from Orion Research Foundation. Karen Peynshaert is a postdoctoral fellow of the Research Foundation-Flanders, Belgium (FWO-Vlaanderen, grant 12Y2719N). We thank

Susanna Boman, Maija Lahtela-Kakkonen and Lea Pirskanen for their help in providing bovine eyes. The Light Microscopy Unit of the Institute of Biotechnology (Hi-LIFE Biocenter Finland infrastructure) at the University of Helsinki is thanked for their help with confocal microscopy.

## Appendix A. Supplementary data

Supplementary data to this article can be found online at https://doi.org/10.1016/j.jconrel.2020.10.028.

## References

[1] R.S. Ramrattan, R.C.W. Wolfs, S. Panda-Jonas, J.B. Jonas, D. Bakker, H.A. Pols, A. Hofman, P.T.V.M. De Jong, Prevalence and causes of visual field loss in the elderly and associations with impairment in daily functioning: the Rotterdam Study, Arch. Ophthalmol. 119 (2001) 1788–1794, https://doi.org/10.1001/archopht.119.12.1788.

[2] K.A. Eckert, M.J. Carter, V.C. Lansingh, D.A. Wilson, J.M. Furtado, K.D. Frick, S. Resnikoff, A simple method for estimating the economic cost of productivity loss due to blindness and moderate to severe visual impairment, Ophthalmic Epidemiol. 22 (2015) 349–355, https://doi.org/10.3109/09286586.2015.1066394.

[3] J. Lee, J. Kim, M. Jeong, H. Lee, U. Goh, H. Kim, B. Kim, J.H. Park, Liposome-based engineering of cells to package hydrophobic compounds in membrane vesicles for tumor penetration, Nano Lett. 15 (2015) 2938–2944, https://doi.org/10.1021/nl5047494.

[4] D.B. Rein, J.S. Wittenborn, X. Zhang, A.A. Honeycutt, S.B. Lesesne, J. Saaddine, Forecasting age-related macular degeneration through the year 2050: the potential impact of new treatments, Arch. Ophthalmol. 127 (2009) 533–540, https://doi.org/10.1001/archophthalmol.2009.58.

[5] E.M. del Amo, A.K. Rimpelä, E. Heikkinen, O.K. Kari, E. Ramsay, T. Lajunen, M. Schmitt, L. Pelkonen, M. Bhattacharya, D. Richardson, A. Subrizi, T. Turunen, M. Reinisalo, J. Itkonen, E. Toropainen, M. Casteleijn, H. Kidron, M. Antopolsky, K. S. Vellonen, M. Ruponen, A. Urtti, Pharmacokinetic aspects of retinal drug delivery, Prog. Retin. Eye Res. 57 (2017) 134–185, https://doi.org/10.1016/j.preteyeres.2016.12.001.

[6] E.M. Del Amo, K.S. Vellonen, H. Kidron, A. Urtti, Intravitreal clearance and volume of distribution of compounds in rabbits: in silico prediction and pharmacokinetic simulations for drug development, Eur. J. Pharm. Biopharm. 95 (2015) 215–226, https://doi.org/10.1016/j.ejpb.2015.01.003.

[7] J. Devoldere, K. Peynshaert, H. Dewitte, C. Vanhove, L. De Groef, L. Moons, S. Y. Özcan, D. Dalkara, S.C. De Smedt, K. Remaut, Non-viral delivery of chemically modified mRNA to the retina: subretinal versus intravitreal administration, J. Control. Release 307 (2019) 315–330, https://doi.org/10.1016/j.jconrel.2019.06.042.

[8] D. Dalkara, K.D. Kolstad, N. Caporale, M. Visel, R.R. Klimczak, D.V. Schaffer, J. G. Flannery, Inner limiting membrane barriers to aav-mediated retinal transduction from the vitreous, Mol. Ther. 17 (2009) 2096–2102, https://doi.org/10.1038/mt.2009.181.

[9] L. Gan, J. Wang, Y. Zhao, D. Chen, C. Zhu, J. Liu, Y. Gan, Hyaluronan-modified core-shell liponanoparticles targeting CD44-positive retinal pigment epithelium cells via intravitreal injection, Biomaterials 34 (2013) 5978–5987, https://doi.org/10.1016/j.biomaterials.2013.04.035.

[10] J. Lee, N. Ryoo, H. Han, H. Kyoung Hong, J. Yeon Park, S. Jun Park, Y.-K. Kim, C. Sim, K. Kim, S. Joon Woo, K. Hyung Park, H. Kim, Anti-VEGF PolysiRNA Polyplex for the Treatment of Choroidal Neovascularization, 2016, https://doi.org/10.1021/acs.molpharmaceut.6b00148.

[11] S.C. Bu, R. Kuijer, R.J. Van Der Worp, X.R. Li, J.M.M. Hooymans, L.I. Los, The ultrastructural localization of type II, IV, and VI collagens at the vitreoretinal interface, PLoS One 10 (2015), https://doi.org/10.1371/journal.pone.0134325.

[12] P.N. Bishop, Structural macromolecules and supramolecular organisation of the vitreous gel, Prog. Retin. Eye Res. 19 (2000) 323–344, https://doi.org/10.1016/S1350-9462(99)00016-6.

[13] B.T. Käsdorf, F. Arends, O. Lieleg, Diffusion regulation in the vitreous humor, Biophys. J. 109 (2015) 2171–2181, https://doi.org/10.1016/j.bpj.2015.10.002.

[14] M.M. Le Goff, P.N. Bishop, Adult vitreous structure and postnatal changes, Eye 22 (2008) 1214–1222, https://doi.org/10.1038/eye.2008.21.

[15] S. Tavakoli, O.K. Kari, T. Turunen, T. Lajunen, M. Schmitt, J. Lehtinen, F. Tasaka, P. Parkkila, J. Ndika, T. Viitala, H. Alenius, A. Urtti, A. Subrizi, Diffusion and Protein Corona Formation of Lipid-based Nanoparticles in Vitreous Humor: Profiling and Pharmacokinetic Considerations, 2020, https://doi.org/10.1021/acs.molpharmaceut.0c00411.

[16] L. Pitkänen, M. Ruponen, J. Nieminen, A. Urtti, Vitreous is a barrier in nonviral gene transfer by cationic lipids and polymers, Pharm. Res. 20 (2003) 576–583, https://doi.org/10.1023/A:1023238530504.

[17] T.F. Martens, D. Vercauteren, K. Forier, H. Deschout, K. Remaut, R. Paesen, M. Ameloot, J.F. Engbersen, J. Demeester, S.C. De Smedt, K. Braeckmans, Measuring the intravitreal mobility of nanomedicines with single-particle tracking microscopy, Nanomedicine 8 (2013) 1955–1968, https://doi.org/10.2217/nnm.12.202.

[18] J. Mains, C.G. Wilson, The vitreous humor as a barrier to nanoparticle distribution, J. Ocul. Pharmacol. Ther. 29 (2013) 143–150, https://doi.org/10.1089/jop.2012.0138.

[19] Q. Xu, N.J. Boylan, J.S. Suk, Y.Y. Wang, E.A. Nance, J.C. Yang, P.J. McDonnell, R. A. Cone, E.J. Duh, J. Hanes, Nanoparticle diffusion in, and microrheology of, the bovine vitreous ex vivo, J. Control. Release 167 (2013) 76–84, https://doi.org/10.1016/j.jconrel.2013.01.018.

[20] J. Sebag, Anatomy and pathology of the vitreo-retinal interface, Eye 6 (1992) 541–552, https://doi.org/10.1038/eye.1992.119.

[21] W. Halfter, P. Oertle, C.A. Monnier, L. Camenzind, M. Reyes-Lua, H. Hu, J. Candiello, A. Labilloy, M. Balasubramani, P.B. Henrich, M. Plodinec, New concepts in basement membrane biology, FEBS J. 282 (2015) 4466–4479, https://doi.org/10.1111/febs.13495.

[22] P.B. Henrich, C.A. Monnier, W. Halfter, C. Haritoglou, R.W. Strauss, R.Y.H. Lim, M. Loparic, Nanoscale topographic and biomechanical studies of the human internal limiting membrane, Invest. Ophthalmol. Vis. Sci. 53 (2012) 2561–2570, https://doi.org/10.1167/iovs.11-8502.

[23] H. Koo, H. Moon, H. Han, J.H. Na, M.S. Huh, J.H. Park, S.J. Woo, K.H. Park, I. Chan Kwon, K. Kim, H. Kim, The movement of self-assembled amphiphilic polymeric nanoparticles in the vitreous and retina after intravitreal injection, Biomaterials 33 (2012) 3485–3493, https://doi.org/10.1016/j.biomaterials.2012.01.030.

[24] E. Ojeda, G. Puras, M. Agirre, J. Zarate, S. Grijalvo, R. Eritja, G. Martinez-Navarrete, C. Soto-Sánchez, A. Diaz-Tahoces, M. Aviles-Trigueros, E. Fernández, J. L. Pedraz, The influence of the polar head-group of synthetic cationic lipids on the transfection efficiency mediated by niosomes in rat retina and brain, Biomaterials 77 (2016) 267–279, https://doi.org/10.1016/j.biomaterials.2015.11.017.

[25] W. Tian, S. Schulze, M. Brandl, G. Winter, Vesicular phospholipid gel-based depot formulations for pharmaceutical proteins: development and in vitro evaluation, J. Control. Release 142 (2010) 319–325, https://doi.org/10.1016/j.jconrel.2009.11.006.

[26] T. Lajunen, L.S. Kontturi, L. Viitala, M. Manna, O. Cramariuc, T. Róg, A. Bunker, T. Laaksonen, T. Viitala, L. Murtomäki, A. Urtti, Indocyanine green-loaded liposomes for light-triggered drug release, Mol. Pharm. 13 (2016) 2095–2107, https://doi.org/10.1021/acs.molpharmaceut.6b00207.

[27] K. Peynshaert, J. Devoldere, V. Forster, S. Picaud, C. Vanhove, S.C. De Smedt, K. Remaut, Toward smart design of retinal drug carriers: a novel bovine retinal explant model to study the barrier role of the vitreoretinal interface, Drug Deliv. 24 (2017) 1384–1394, https://doi.org/10.1080/10717544.2017.1375578.

[28] V. Sarao, D. Veritti, F. Boscia, P. Lanzetta, Intravitreal Steroids for the Treatment of Retinal Diseases, 2014, https://doi.org/10.1155/2014/989501.

[29] M.W. Stewart, S. Grippon, P. Kirkpatrick, Aflibercept, Nat. Rev. Drug Discov. 114 (11) (2012) 269–270, https://doi.org/10.1038/nrd3700.

[30] R. Narayanan, B.D. Kuppermann, C. Jones, P. Kirkpatrick, Ranibizumab, Nat. Rev. Drug Discov. 5 (2006) 815–816, https://doi.org/10.1038/nrd2157.

[31] W. Halfter, S. Dong, A. Dong, A.W. Eller, R. Nischt, Origin and turnover of ECM proteins from the inner limiting membrane and vitreous body, in: Eye, Nature Publishing Group, 2008, pp. 1207–1213, https://doi.org/10.1038/eye.2008.19.

[32] L. Pitkänen, J. Pelkonen, M. Ruponen, S. Rönkkö, A. Urtti, Neural retina limits the nonviral gene transfer to retinal pigment epithelium in an in vitro bovine eye model, AAPS J. 6 (2004) 72–80, https://doi.org/10.1208/aapsj060325.

[33] K. Peynshaert, J. Devoldere, A.K. Minnaert, S.C. De Smedt, K. Remaut, Morphology and composition of the inner limiting membrane: species-specific variations and relevance toward drug delivery research, Curr. Eye Res. 44 (2019) 465–475, https://doi.org/10.1080/02713683.2019.1565890.

[34] S. Shafaie, V. Hutter, M.B. Brown, M.T. Cook, D.Y.S. Chau, Diffusion through the ex vivo vitreal body – bovine, porcine, and ovine models are poor surrogates for the human vitreous, Int. J. Pharm. 550 (2018) 207–215, https://doi.org/10.1016/j.ijpharm.2018.07.070.

[35] J. Xu, J.J. Heys, V.H. Barocas, T.W. Randolph, Permeability and diffusion in vitreous humor: implications for drug delivery, Pharm. Res. 17 (2000) 664–669, https://doi.org/10.1023/A:1007517912927.

[36] C.S. Nickerson, J. Park, J.A. Kornfield, H. Karageozian, Rheological properties of the vitreous and the role of hyaluronic acid, J. Biomech. 41 (2008) 1840–1846, https://doi.org/10.1016/j.jbiomech.2008.04.015.

[37] R.S. Matsumoto, J.C. Blanks, Topographic variations in the rabbit and primate internal limiting membrane, Invest. Ophthalmol. Vis. Sci. 25 (1984) 71–82.

[38] S. Heegaard, Structure of the human vitreoretinal border region, Ophthalmologica 208 (1994) 82–91, https://doi.org/10.1159/000310458.

[39] J. Candiello, G.J. Cole, W. Halfter, Age-dependent changes in the structure, composition and biophysical properties of a human basement membrane, Matrix Biol. 29 (2010) 402–410, https://doi.org/10.1016/j.matbio.2010.03.004.

[40] W. Halfter, J. Sebag, E.T. Cunningham, Vitreoretinal interface and inner limiting membrane, in: Vitr. Heal. Dis, Springer New York, 2014, pp. 165–191, https://doi.org/10.1007/978-1-4939-1086-1_11.

[41] K. Peynshaert, J. Devoldere, S.C. De Smedt, K. Remaut, In vitro and ex vivo models to study drug delivery barriers in the posterior segment of the eye, Adv. Drug Deliv. Rev. 126 (2018) 44–57, https://doi.org/10.1016/j.addr.2017.09.007.

[42] J.L. Bourges, S.E. Gautier, F. Delie, R.A. Bejjani, J.C. Jeanny, R. Gurny, D. BenEzra, F.F. Behar-Cohen, Ocular drug delivery targeting the retina and retinal pigment epithelium using polylactide nanoparticles, Investig. Ophthalmol. Vis. Sci. 44 (2003) 3562–3569, https://doi.org/10.1167/iovs.02-1068.

[43] E. Sakurai, H. Ozeki, N. Kunou, Y. Ogura, Effect of particle size of polymeric nanospheres on intravitreal kinetics, Ophthalmic Res. 33 (2001) 31–36, https://doi.org/10.1159/000055638.

[44] J. Lee, U. Goh, H.-J. Lee, J. Kim, M. Jeong, J.-H. Park, Effective Retinal Penetration of Lipophilic and Lipid-conjugated Hydrophilic Agents Delivered by Engineered Liposomes, 2016, https://doi.org/10.1021/acs.molpharmaceut.6b00864.

[45] T.L. Jackson, R.J. Antcliff, J. Hillenkamp, J. Marshall, Human retinal molecular weight exclusion limit and estimate of species variation, Investig. Ophthalmol. Vis. Sci. 44 (2003) 2141–2146, https://doi.org/10.1167/iovs.02-1027.
[46] A. Popov, E.M. Enlow, H. Chen, Compositions and Methods for Ophthalmic and/or Other Applications. https://patents.google.com/patent/US9827191B2/en, 2017.
[47] J. Devoldere, M. Wels, K. Peynshaert, H. Dewitte, S.C. De Smedt, K. Remaut, The obstacle course to the inner retina: hyaluronic acid-coated lipoplexes cross the vitreous but fail to overcome the inner limiting membrane, Eur. J. Pharm. Biopharm. 141 (2019) 161–171, https://doi.org/10.1016/j.ejpb.2019.05.023.
[48] J. Qu, D. Wang, C.L. Grosskreutz, Mechanisms of retinal ganglion cell injury and defense in glaucoma, Exp. Eye Res. 91 (2010) 48–53, https://doi.org/10.1016/j.exer.2010.04.002.
[49] E. Fröhlich, The role of surface charge in cellular uptake and cytotoxicity of medical nanoparticles, Int. J. Nanomedicine 7 (2012) 5577–5591, https://doi.org/10.2147/IJN.S36111.
[50] H. Kim, S.B. Robinson, K.G. Csaky, Investigating the movement of intravitreal human serum albumin nanoparticles in the vitreous and retina, Pharm. Res. 26 (2009) 329–337, https://doi.org/10.1007/s11095-008-9745-6.
[51] N. Pippa, C. Demetzos, S. Pispas, C. Demetzos, S. Pispas, Drug Delivery Nanosystems, Jenny Stanford Publishing, 2019, https://doi.org/10.1201/9780429490545.
[52] R. Ridolfo, S. Tavakoli, V. Junnuthula, D.S. Williams, A. Urtti, J.C.M. van Hest, Exploring the impact of morphology on the properties of biodegradable nanoparticles and their diffusion in complex biological medium, Biomacromolecules (2020), https://doi.org/10.1021/acs.biomac.0c00726.